

---

# What Are Good Positional Encodings for Directed Graphs?

---

**Yinan Huang**

Georgia Institute of Technology  
yhuang903@gatech.edu

**Haoyu Wang**

Georgia Institute of Technology  
haoyu.wang@gatech.edu

**Pan Li**

Georgia Institute of Technology  
panli@gatech.edu

## Abstract

Positional encodings (PE) for graphs are essential in constructing powerful and expressive graph neural networks and graph transformers as they effectively capture relative spatial relations between nodes. While PEs for undirected graphs have been extensively studied, those for directed graphs remain largely unexplored, despite the fundamental role of directed graphs in representing entities with strong logical dependencies, such as those in program analysis and circuit designs. This work studies the design of PEs for directed graphs that are expressive to represent desired directed spatial relations. We first propose *walk profile*, a generalization of walk counting sequence to directed graphs. We identify limitations in existing PE methods—including symmetrized Laplacian PE, Singular Value Decomposition PE, and Magnetic Laplacian PE—in their ability to express walk profiles. To address these limitations, we propose the *Multi-q Magnetic Laplacian* PE, which extends Magnetic Laplacian PE with multiple potential factors. This simple variant turns out to be capable of provably expressing walk profiles. Furthermore, we generalize previous basis-invariant and stable networks to handle complex-domain PEs decomposed from Magnetic Laplacians. Our numerical experiments demonstrate the effectiveness of Multi-q Magnetic Laplacian PE with a stable neural architecture, outperforming previous PE methods (with stable networks) on predicting directed distances/walk profiles, sorting network satisfiability, and on general circuit benchmarks. Our code is available at <https://github.com/Graph-COM/Multi-q-Maglap>.

## 1 Introduction

Positional encoding (PE) [49, 53], which refers to the vectorized representation of token positions within a series of tokens, has been widely integrated into modern deep learning models across various data modalities, such as language modeling [53], vision tasks [18], and graph learning [19, 45]. The key advantage of PE is its ability to preserve crucial positional information of tokens, thereby complementing many downstream position-agnostic models like transformers [61] and graph neural networks (GNNs) [34, 37]. For regularly ordered data, such as sequences or images, defining PE is relatively straightforward; for instance, one can use sinusoidal functions of varying frequencies (known as Fourier features) as PE [53]. In contrast, designing PE for structured graph data is more challenging due to the lack of canonical node ordering in graphs.

There have been significant efforts dedicated to designing effective positional encodings (PEs) for graphs [5, 19, 20, 33, 35, 37, 45, 55]. It is particularly interesting because graph PEs can

be used for building powerful graph transformers as well as improving the expressive power of GNNs [35, 37, 55]. In particular, Laplacian positional encoding (Lap-PE) [19, 33], as one of the most fundamental PEs for **undirected graphs**, is adopted by many state-of-the-art graph machine learning models [10, 27, 37, 45]. The eigenvalue decomposition nature of Lap-PE makes it a strong candidate since eigenvalues and eigenvectors fully preserve the graph structure information and can express various distances defined on graphs, such as shortest path distance [56], diffusion distance [9, 13], resistance distance [59] and biharmonic distance [33, 38]. Lap-PE is also well understood in the context of graph spectrum theory [12].

Despite the success of Lap-PEs for undirected graphs, many real-world applications involve **directed graphs**, e.g., circuit designs, program analysis, neural architecture search, citation network, financial network, etc [4, 7, 39, 43, 46, 54, 57, 62, 66]. The direction of edges in these graphs carries important semantic meanings that cannot be overlooked. For instance, in data-flow analysis, a program can be parsed as a data-flow graph [8, 15]. Analysis of reachability, liveness and common subexpressions requires understanding node dependencies in both forward and backward directions [14, 15]; in digital circuit timing analysis, one key problem is to find the directed path between the input nodes and the output nodes with maximal delay, known as the critical path [11]; in logical reasoning, one also needs to identify directed dependence between entities, such as common successors/predecessors or even higher-hop relations [44, 51]. These examples underscore the significance of a model’s ability to encode the intricate nature of directed relations effectively.

However, how to properly define effective PEs for directed graphs to capture these complicated directed relations is open. One big technical challenge is that the Laplacian matrix is no longer symmetric, making eigenvalues and eigenvectors complex numbers, and eigenvectors are not necessarily orthogonal. As a result, Lap-PE may not be a good PE candidate for directed graphs. Accordingly, there have been considerable attempts to deal with the asymmetry in matrix factorization (e.g., symmetrized Laplacian PE [19], singular value decomposition PE (SVD-PE) [28], Magnetic Laplacian PE (Mag-PE) [25]). Nevertheless, no work has been done to analyze whether these induced PEs are expressive enough to represent the desired directed relations.

In this work, we study the expressive power of PEs for directed graphs in terms of encoding directed relation. Our main contributions include:

- We propose a notation of directed relations named *walk profile*, which generalizes undirected walk counting to directed graphs. Walk profile is an array whose entries describe the number of bidirectional walks with a specific number of forward and backward edges. Common distance notations such as directed shortest(longest) path distance can be read out from the walk profile.
- We find that symmetrized Laplacian PE, SVD-PE, and Mag-PE fail to determine walk profile. To address this problem, we propose a simple yet effective PE called Multi-q Magnetic Laplacian PE (Multi-q Mag-PE), which jointly takes eigenvalues and eigenvectors factorized from multiple Magnetic Laplacian with different potential  $q$ ’s. We prove that the resulting PEs can reconstruct walk profile, leading to stronger distance representation power. The key insight here is that  $q$  serves as the frequency of phase shift that records the bidirectional walks on the graph, and using multiple frequencies  $q$  allows us to fully reconstruct walk information by Fourier transform.
- Besides, to handle the non-uniqueness of Magnetic Laplacian decomposition, we generalize the previous basis-invariant and stable neural architecture [27, 55], from real domain to handle complex eigenvectors. The invariant property ensures that two equivalent complex eigenvectors (e.g., differ in a complex basis transformation) have the same representations. Moreover, the stability allows bridging Lap-PE (potential  $q = 0$ ) and Mag-PE (potential  $q \neq 0$ ) smoothly.
- We implement PEs from symmetric Laplacian, SVD, Magnetic Laplacian and the proposed multi-q Magnetic Laplacian, equipped with basis-invariant and stable architectures. Empirical results on synthetic datasets (distance prediction, sorting network satisfiability prediction) demonstrate the stronger power of multi-q Mag-PEs to encode directedness. Real-world tasks (analog circuits prediction, high-level synthetic) show the constant performance gain of using multi-q Mag-PEs compared to existing PE methods.

## 2 Related Works

**Neural networks for directed graphs.** Neural networks for directed graphs can be mainly categorized into three types: spatial GNNs, spectral GNNs, and transformers. Spatial GNNs are those who

directly use graph topology as the inductive bias in model design, including bidirectional message passing neural networks [29, 32, 57] for general directed graphs and asynchronous message passing exclusively for directed acyclic graphs [17, 50, 63]. Spectral GNNs aim to generalize the concepts of Fourier basis, Fourier transform and the corresponding spectral convolution from undirected graphs to directed graphs. Potential choices include Magnetic Laplacian [23, 24, 26, 65], Jordan decomposition [48], Perron eigenvectors [41], motif Laplacian [42], Proximity matrix [52] and direct generalization by holomorphic functional calculus [31]. Finally, transformer-based models adopt the attention mechanism and their core ideas are to devise direction-aware positional encodings that better indicate graph structural information [25, 28], which are reviewed next.

**Positional encodings for undirected/directed graphs.** Many works focus on designing positional encodings (PE) for undirected graphs, e.g., Laplacian-based PE [5, 19, 27, 33, 37, 55], random walk PE [20, 35]. See [45] for a survey and [6] for a study on the relation between different types of PEs. On the other hand, recently there have been many efforts to generalize PE to directed graphs. Symmetrized Laplacian symmetrizes the directed graph into an undirected one and applies regular undirected Laplacian PE [19]. Singular vectors of the asymmetric adjacency matrix have also been used as PE [28], and so have the eigenvectors of the Magnetic Laplacian and bidirectional random walks [25]. For directed acyclic graphs, a depth-based positional encoding has been used [40].

### 3 Preliminaries

**Basic notation.** We denote the real domain by  $\mathbb{R}$ , the complex domain by  $\mathbb{C}$  and all integers by  $\mathbb{Z}$ . Bold-face letters such as  $\mathbf{A}$  are used to denote matrices.  $\mathbf{A}^\dagger$  denotes the conjugate transpose of  $\mathbf{A}$ . We use  $i = \sqrt{-1}$  to represent the imaginary unit and  $\mathbf{I}$  for the identity matrix.

**Directed graphs.** Let  $\mathcal{G} = (\mathcal{V}, \mathcal{E})$  be a directed graph, where  $\mathcal{V}$  is the node set and  $\mathcal{E} \subset \mathcal{V} \times \mathcal{V}$  is the edge set. We call  $u$  predecessor of  $v$  if  $(u, v) \in \mathcal{E}$  and call  $u$  successor of  $v$  if  $(v, u) \in \mathcal{E}$ .

**Graph symmetrized Laplacian and Magnetic Laplacian.** Let  $\mathbf{A} \in \mathbb{R}^{n \times n}$  be the adjacency matrix of a directed graph with  $n$  nodes where  $A_{u,v} = 1$  if  $(u, v) \in \mathcal{E}$  and 0 otherwise. Denote  $\mathbf{D}$  as the diagonal node degree matrix where  $D_{u,u}$  is the in-degree  $d_{\text{in},u}$  plus the out-degree  $d_{\text{out},u}$  of node  $u$ . *Magnetic Laplacian*  $\mathbf{L}_q$ , with a parameter  $q \in \mathbb{R}$  called potential, is defined by  $\mathbf{L}_q = \mathbf{I} - \mathbf{D}^{-1/2} \mathbf{A}_q \mathbf{D}^{-1/2}$ , where  $\mathbf{A}_q \in \mathbb{C}^{n \times n}$  is defined by

$$[\mathbf{A}_q]_{u,v} = \begin{cases} \exp\{i2\pi q\}, & \text{if } (u, v) \in \mathcal{E}, \\ \exp\{-i2\pi q\}, & \text{if } (v, u) \in \mathcal{E}, \\ 1, & \text{if } (u, v), (v, u) \in \mathcal{E}, \end{cases} \quad (1)$$

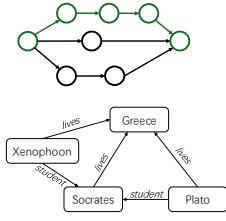
$\mathbf{L}_q$  encodes edge directions via the phases of complex numbers  $\exp\{\pm i2\pi q\}$ . As a generalization of Laplacian on undirected graphs,  $\mathbf{L}_q$  is widely studied in applied mathematics, physics and network science for directed graph analysis [21, 22, 47], and are recently introduced as a promising way to build graph filters and deep learning models for directed graphs [23, 24, 25, 26]. *Symmetrized Laplacian*  $\mathbf{L}_s (= \mathbf{L}_{q=0})$  is essentially a special case of Magnetic Laplacian with potential  $q = 0$  (no phase difference). Magnetic Laplacian  $\mathbf{L}_q$  is hermitian since  $\mathbf{L}_q^\dagger = \mathbf{L}_q$ . This implies that there exists eigendecomposition  $\mathbf{L}_q = \mathbf{V} \mathbf{\Lambda} \mathbf{V}^\dagger$ , where  $\mathbf{V} \in \mathbb{C}^{n \times n}$  is a unitary matrix, and  $\mathbf{\Lambda} = \text{diag}(\boldsymbol{\lambda})$  constitutes of real eigenvalues  $\boldsymbol{\lambda} \in \mathbb{R}^n$ . The Magnetic Laplacian PE of node  $u$  is defined by the corresponding row of  $\mathbf{V}$ , denoted by  $z_u = [\mathbf{V}_{u,:}]^\top$ .

## 4 What Are Good Positional Encodings for Directed Graphs?

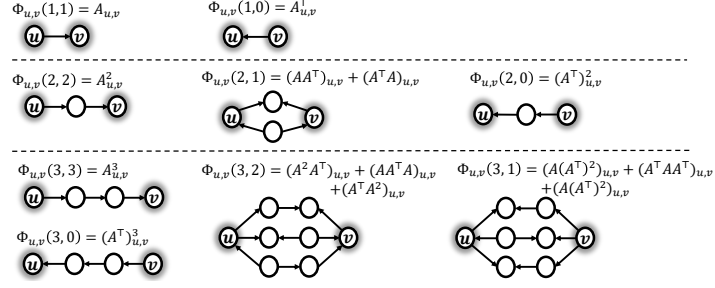
In this section, we are going to study the capability of existing directional PEs to encode directed relations. We first define a generic notation that collects directed relational information on directed graphs. Importantly, this notation should be *bidirectional*, i.e., considering following or reversing the edge directions, in order to represent relations such as common successors/predecessors. Meanwhile, it should be able to express distance metrics such as shortest/longest path distances.

### 4.1 Walk Profile: a General Notation for Directed Relations

On undirected graphs, one way to describe the spatial relation between node  $u$  and  $v$  is through walk counting sequences at different lengths  $\mathcal{W}_{u,v} = (\mathbf{A}_{u,v}, \mathbf{A}_{u,v}^2, \mathbf{A}_{u,v}^3, \dots, \mathbf{A}_{u,v}^L)$ . In particular, suppose



(a) Upper: critical path (green) as the longest path. Lower: logical reasoning



(b) Examples of Walk profile from node  $u$  to  $v$ .

$A \in \{0, 1\}^{n \times n}$ , then  $A_{u,v}^\ell$  counts the number of  $\ell$ -length walks from  $u$  to  $v$  and the shortest path distance can be found by  $spd_{u,v} = \min\{\ell : A_{u,v}^\ell > 0\}$ . For directed graphs, we can adopt the same description with  $A$  replaced by the asymmetric adjacency matrix. However, this single-directional walk could miss important distance information on directed graphs. For example, consider a directed graph with  $E = \{(1, 3), (2, 3)\}$ . As we cannot reach node 2 from node 1, the walk counting from node 2 to node 1 is always zero. But clearly these two nodes share a common successor node 3 and their relation is more than simply saying “they are not reachable to each other”.

A key observation is that inference of common successor/predecessor requires knowing  $AA^\top$  and  $A^\top A$  instead of simply power of  $A$ . This motivates us to define walk counting in a **bidirectional** manner. In other words, one is able to walk using both  $A$  and  $A^\top$  in a walk. Therefore, we introduce bidirectional walks which consider combinations of  $A$  and  $A^\top$ .

**Definition 4.1** (Bidirectional Walk). *Let  $\mathcal{G} = (\mathcal{V}, \mathcal{E})$  be a directed graph. A bidirectional walk  $w = (v_0, v_1, v_2, \dots)$  is a sequence of nodes where every consecutive two nodes form either a forward edge  $(v_i, v_{i+1}) \in \mathcal{E}$  or a backward edge  $(v_{i+1}, v_i) \in \mathcal{E}$ . The length of a bidirectional walk is the total number of forward edges and backward edges it contains.*

As two bidirectional walks of the same length could have different numbers of forward edges and backward edges, we introduce the notion of *Walk Profile*, a generalization of walk counting that counts and categorizes bidirectional walks by its number of forward edges and backward edges.

**Definition 4.2** (Walk Profile). *Let  $\mathcal{G}$  be a directed graph and  $A$  be the adjacency matrix. Given two nodes  $u, v$ , Walk profile  $\Phi_{u,v}(\ell, k)$  is the number of length- $\ell$  bidirectional walks from  $u$  to  $v$  that contains exact  $k$  forward edges and  $\ell - k$  backward edges. Mathematically,*

$$\Phi_{u,v}(\ell, k) = \sum_{A_i \in \{A, A^\top\}, k \text{ of } A_1, \dots, A_\ell \text{ is } A} [A_1 A_2 \dots A_\ell]_{u,v} \quad (2)$$

This definition can be applied for general weighted adjacency matrix  $A \in \mathbb{R}^{n \times n}$  or  $A \in \mathbb{C}^{n \times n}$ .

For example,  $\Phi_{u,v}(1, 1)$  represents the adjacency from  $u$  to  $v$ ;  $\Phi_{u,v}(2, 1) = (AA^\top)_{u,v} + (A^\top A)_{u,v}$ , which counts the number 2-length walk with one forward edge and one backward edge, which corresponds to the number of common successors and common predecessors in total. One can also compute the shortest/longest path distance using the walk profile.

**Remark 4.1.** *Let  $\mathcal{G}$  be a directed graph with Adjacency matrix  $A \in \{0, 1\}^{n \times n}$ , and consider two nodes  $u, v$ . The shortest path distance can be computed via  $spd_{u,v} = \min\{\ell \in \mathbb{Z} : \Phi_{u,v}(\ell, \ell) > 0\}$ . Furthermore, if  $\mathcal{G}$  is acyclic, then longest path distance is  $lpd_{u,v} = \max\{\ell \in \mathbb{Z} : \Phi_{u,v}(\ell, \ell) > 0\}$ .*

## 4.2 The Limitations of Existing PEs to Express Walk Profile

Intuitively, a good PE can characterize the distance between two nodes  $u$  and  $v$  based on their PEs  $z_u, z_v$ . Now let us study the power of the existing PEs for directed graphs via the notion of walk profile. Formally, we say a PE method is expressive if it can **determine  $\Phi_{u,v}$  based on  $z_u$  and  $z_v$** .

**Mag-PE.** Let  $L_q$  be Magnetic Laplacian with potential  $q$  and the induced positional encodings are  $\{z_u\}_{u \in \mathcal{V}}$  (see Section 3). Since Magnetic Laplacian  $L_q$  faithfully represents the directed structure of the graph, one may naturally conjecture that Mag-PE should be able to compute the walk profile.

However, it turns out that it is impossible to recover  $\Phi_{u,v}(m, k)$  from the Magnetic Laplacian's eigenvalues  $\lambda$  and eigenvectors  $z_u, z_v$ , as shown in the following Theorem 4.1.

**Theorem 4.1.** Fix a  $q \in \mathbb{R}$ . There exist graphs  $\mathcal{G}, \mathcal{G}'$  with adjacency matrices  $\mathbf{A}, \mathbf{A}' \in \mathbb{C}^{n \times n}$ , and nodes  $u, v \in V_{\mathcal{G}}$  and  $u', v' \in V_{\mathcal{G}'}$ , such that  $\text{Mag-PE}(\lambda, z_u, z_v) = (\lambda', z_{u'}, z_{v'})$ , but  $\Phi_{u,v}(m, k) \neq \Phi_{u',v'}(m, k)$  for some  $m, k$ .

**Remark 4.2.** From the formal proof of Theorem 4.1 (see Appendix A) we can also show that Mag-PE of node  $u, v$  is unable to compute shortest path distance  $\text{spd}_{u,v}$ . More insights into why single  $q$  may fail are to be discussed after the proof sketch of Theorem 4.2. Besides, as symmetrized Laplacian can be seen as a special case of Magnetic Laplacian ( $q = 0$ ), the same negative results apply for symmetrized Laplacian PE.

**SVD-PE.** Singular vectors of the asymmetric adjacency matrix may also be used as directed PE [28]. That is,  $\mathbf{A} = \mathbf{U} \text{diag}(\sigma) \mathbf{W}^\top$  and define SVD-PE  $z_u := (\mathbf{U}_{u,:}, \mathbf{W}_{u,:})^\top$ . Here, we provide an intuition on why SVD-PE is hard to construct the walk profile. Recall that in eigen-decomposition, a power series of  $\mathbf{A}$  can be computed via power series of eigenvalues, i.e.,  $f(\mathbf{A}) = \sum_p a_p \mathbf{A}^p = \mathbf{V} \text{diag}[f(\lambda)] \mathbf{V}^\top$ , which explains the distance as a function  $f(\mathbf{A})_{u,v}$  can be expressed by  $\langle \mathbf{V}_{u,:}, f(\lambda) \odot \mathbf{V}_{v,:} \rangle$ . In contrast, this property does not hold for SVD. For instance,  $\mathbf{A}^2 = \mathbf{U} \text{diag}(\sigma) \mathbf{W}^\top \mathbf{U} \text{diag}(\sigma) \mathbf{W}^\top \neq \mathbf{U} \text{diag}(\sigma^2) \mathbf{W}^\top$ . As a result, computation of  $[\mathbf{A}^2]_{u,v}$  (the walk profile more broadly) requires not only SVD-PEs  $z_u, z_v$  but also  $z_w$  for some  $w \in \mathcal{V} \setminus \{u, v\}$ .

### 4.3 Magnetic Laplacian with Multiple Potentials $q$

The limited expressivity of existing PE methods motivates us to design a more powerful direction-aware PE. The limitation of Mag-PE comes from the fact that the accumulated phase shifts over all bidirectional walks by Magnetic Laplacian cannot uniquely determine the number of walks. For example, suppose  $q = 1/8$ , both of the following cases: (1) node  $v$  is not reachable from  $u$ ; (2)  $u \rightarrow u_1 \rightarrow v$  and  $u \leftarrow u_2 \leftarrow v$  yield the same  $[\mathbf{L}_q^\ell]_{u,v} = 0$  for any integer  $\ell$ . However, the numbers of length- $\ell$  walks between  $u$  and  $v$  are different. The potential  $q$  acts like a frequency that records the accumulated phase shift for a walk, and one single frequency  $q$  cannot faithfully decode the distance.

Therefore, we propose *Multi- $q$  Magnetic Laplacian PE (Multi- $q$  Mag-PE)*, which leverages multiple Magnetic Laplacians with different  $q$ 's simultaneously. A  $q$  vector denoted by  $\vec{q} = (q_1, \dots, q_Q)$  is going to construct  $Q$  many Magnetic Laplacian  $\mathbf{L}_{q_1}, \dots, \mathbf{L}_{q_Q}$ , and Multi- $q$  Mag-PE is defined by

$$z_u^{\vec{q}} = ([\mathbf{V}_{q_1}]_{u,:}, \dots, [\mathbf{V}_{q_Q}]_{u,:}), \quad (3)$$

where  $\mathbf{V}_{q_i}$  is the eigenvectors of  $\mathbf{L}_{q_i} = \mathbf{V}_{q_i} \text{diag}(\lambda_{q_i}) \mathbf{V}_{q_i}^\dagger$ . Intuitively, different frequencies (i.e., potential  $q$ ) give a spectrum of phase shifts and we can decode spatial distances from them in a lossless manner. Indeed, the following Theorem 4.2 states that, with a proper number of  $q$ 's, one is able to exactly compute the walk profile of the desired length.

**Theorem 4.2.** Let  $L$  be a positive integer. If we let  $\vec{q} = (q_1, q_2, \dots, q_{L+1})$  with  $L+1$  distinct  $q$ 's and  $q_1, \dots, q_{L+1} \in [0, \frac{1}{2})$ , then for all  $\ell \leq L$  and  $k \leq \ell$ , walk profile  $\Phi_{u,v}(\ell, k)$  can be computed from  $(\lambda^{\vec{q}}, z_u^{\vec{q}}, z_v^{\vec{q}})$ , where  $\lambda^{\vec{q}}, z_u^{\vec{q}}$  are concatenation of eigenvalues/eigenvectors of different  $q$  from  $\vec{q}$ .

*Proof Sketch.* Fix two nodes  $u, v$ . As from  $(\lambda^{\vec{q}}, z_u^{\vec{q}}, z_v^{\vec{q}})$ , we can construct  $[\mathbf{A}_q^\ell]_{u,v}$  for any  $q$ . So the question becomes how we can determine the walk profile  $\Phi_{u,v}(\cdot, \cdot)$  from  $[\mathbf{A}_q^\ell]_{u,v}$ . By definition of walk profile, one can find the following key formula that relates walk profile with  $\mathbf{A}_q^\ell$ : For any  $q$ ,

$$[\mathbf{A}_q^\ell]_{u,v} = e^{-i2\pi q \ell} \sum_{k=0}^{\ell} \Phi_{u,v}(\ell, k) e^{i4\pi q k}. \quad (4)$$

Fix the integer  $L$  and consider a length- $Q$  list of  $q$  denoted by  $\vec{q} = (q_1, \dots, q_Q)$ . Then, by Eq. (4), given  $[\mathbf{A}_{q_1}^\ell]_{u,v}, \dots, [\mathbf{A}_{q_Q}^\ell]_{u,v}$  for all  $\ell \leq L$ , solving  $\Phi_{u,v}(\ell, k)$  is equivalent to solving a linear system  $\mathbf{F}\Phi = \mathbf{Y}$ , where  $\mathbf{F} \in \mathbb{C}^{Q \times (L+1)}$ ,  $\Phi \in \mathbb{R}^{(L+1) \times L}$ ,  $\mathbf{Y} \in \mathbb{C}^{Q \times L}$  and  $\mathbf{F}_{j,m} = \exp\{i4\pi q_j m\}$ ,  $\Phi_{j,m} = \Phi_{u,v}(m, j)$  (equals zero if  $j > m$ ),  $\mathbf{Y}_{j,m} = [\mathbf{A}_{q_j}^m]_{u,v} \cdot e^{i2\pi q_j m}$ . To ensure we can uniquely solve the walk profile  $\Phi$  from  $\mathbf{Y}$  in this linear system, we require  $Q = L+1$ , and  $e^{i4\pi q_i} \neq e^{i4\pi q_j}$  for any  $i \neq j$ . The later can be satisfied when  $q_i \in [0, \frac{1}{2})$  and  $q_i \neq q_j$  for all  $i \neq j$ . Indeed, we can let

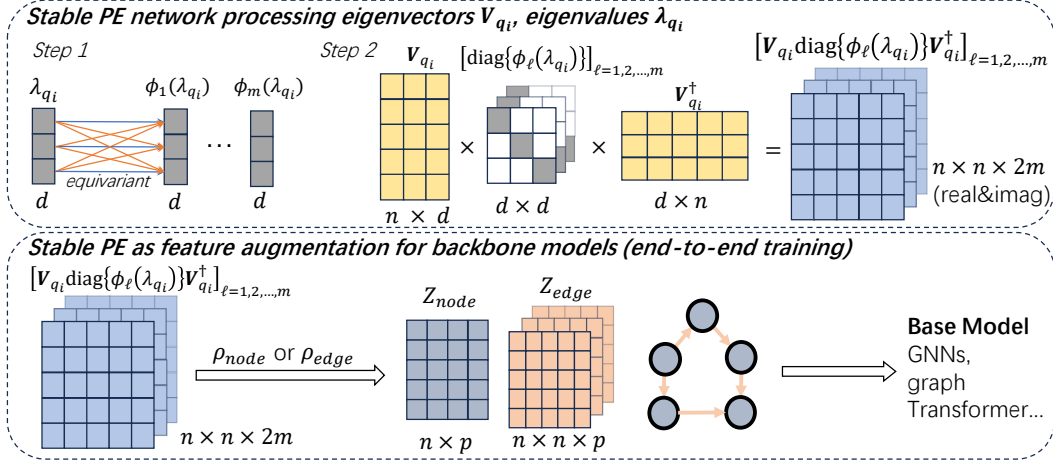


Figure 2: Multi-q Magnetic Laplacian under stable PE framework. Eigenvectors and eigenvalues of each Magnetic Laplacian with different  $q$  will be processed independently and identically and concatenated in the end.

$\vec{q} = (\frac{0}{2(L+1)}, \dots, \frac{L}{2(L+1)})$ , then  $F$  matrix becomes **discrete Fourier transform**, which is a full-rank unitary matrix. It implies we can uniquely determine walk profile  $\Phi_{u,v}(\ell, k)$  for  $\ell \leq L$  based on  $Y$ . Since multi-q Mag-PE enables us to construct  $Y$ , we finish the proof.  $\square$

The proof also provides insights into the issue of using single  $q$ : determining the walk profile from powers of  $A_q$  for a single  $q$  is ill-posed. In contrast, using  $L + 1$  many  $q$ 's simultaneously makes the problem well-posed and allows it to uniquely determine the walk profile of length  $\leq L$ . The number of  $q$  can be interpreted and chosen based on the walk length we are interested in for a specific task.

#### 4.4 Basis-invariant/stable neural architecture for complex eigenvectors

Recent studies have shown that Lap-PE has the issues of basis ambiguity and instability [6, 27, 37, 55]. That is, because eigen-decomposition is not unique (i.e.,  $L = V\Lambda V^\top = (VQ)\Lambda(VQ)^\top$  for some orthogonal matrix  $Q$ ), Lap-PE can become completely different for the same Laplacian and more generally be unstable to Laplacian perturbation. Similar problems still exist for Mag-PE. In fact, they become technically harder because Mag-PEs live in the complex domain and the basis ambiguity extends to unitary basis transform:  $L_q = V\Lambda V^\dagger = (VQ)\Lambda(VQ)^\dagger$  for some unitary matrix  $Q \in \mathbb{C}^{n \times n}$ . For Multi-q Mag-PE, eigenvectors associated with each  $q$  exhibit their own symmetry, exacerbating the ambiguity and stability issues even further.

To address this problem, we aim to generalize the previous stable PE frameworks, PEG [55] and SPE [27], to handle complex eigenvectors. Our framework will process PEs into stable representations and use them as augmented node/edge features in the backbone model. We first consider Mag-PE of a single  $q$  and then extend it. Specifically, let  $\phi_\ell^{\text{node}}, \phi_\ell^{\text{edge}} : \mathbb{R}^d \rightarrow \mathbb{R}^d$  be permutation-equivariant function w.r.t.  $d$ -dim axis (i.e., equivariant to permutation of eigenvalues), we can construct node-level stable PE  $z_{\text{node}} \in \mathbb{R}^{n \times d}$  or edge-level stable PE  $z_{\text{edge}} \in \mathbb{R}^{n \times n \times d}$  in the following ways:

$$z_{\text{node}} = \rho_{\text{node}}(\text{Re}\{V \text{diag}(\phi_1^{\text{node}}(\lambda)) V^\dagger\}, \dots, \text{Re}\{V \text{diag}(\phi_m^{\text{node}}(\lambda)) V^\dagger\}, \\ \text{Im}\{V \text{diag}(\phi_1^{\text{node}}(\lambda)) V^\dagger\}, \dots, \text{Im}\{V \text{diag}(\phi_m^{\text{node}}(\lambda)) V^\dagger\}), \quad (5)$$

$$z_{\text{edge}} = \rho_{\text{edge}}(\text{Re}\{V \text{diag}(\phi_1^{\text{edge}}(\lambda)) V^\dagger\}, \dots, \text{Re}\{V \text{diag}(\phi_m^{\text{edge}}(\lambda)) V^\dagger\}, \\ \text{Im}\{V \text{diag}(\phi_1^{\text{edge}}(\lambda)) V^\dagger\}, \dots, \text{Im}\{V \text{diag}(\phi_m^{\text{edge}}(\lambda)) V^\dagger\}), \quad (6)$$

where  $V, \lambda$  are the eigenvectors and eigenvalues of Magnetic Laplacian with a certain  $q$ ,  $\text{Re}\{\cdot\}, \text{Im}\{\cdot\}$  means taking the real and imaginary parts, respectively, and  $\rho_{\text{node}} : \mathbb{R}^{n \times n \times 2m} \rightarrow \mathbb{R}^{n \times p}$  and  $\rho_{\text{edge}} : \mathbb{R}^{n \times n \times 2m} \rightarrow \mathbb{R}^{n \times n \times p}$  are permutation equivariant function w.r.t.  $n$ -dim axis (i.e., equivariant to permutation of node indices). Afterwards,  $z_{\text{node}}$  will be concatenated with node features, and  $z_{\text{edge}}$  will be concatenated with edge features.

Table 1: Test RMSE results over 3 random seeds for node-pair distance prediction.

| PE method          | PE processing | Directed Acyclic Graph            |                                   |                                   | Regular Directed Graph            |                                   |                                   |
|--------------------|---------------|-----------------------------------|-----------------------------------|-----------------------------------|-----------------------------------|-----------------------------------|-----------------------------------|
|                    |               | <i>spd</i>                        | <i>lpd</i>                        | <i>wp(4, ·)</i>                   | <i>spd</i>                        | <i>lpd</i>                        | <i>wp(4, ·)</i>                   |
| Lap                | Naive         | 0.488 $\pm$ 0.005                 | 0.727 $\pm$ 0.005                 | 1.707 $\pm$ 0.019                 | 2.068 $\pm$ 0.004                 | 1.898 $\pm$ 0.001                 | 2.699 $\pm$ 0.015                 |
|                    | SignNet       | 0.537 $\pm$ 0.013                 | 0.771 $\pm$ 0.013                 | 1.924 $\pm$ 0.002                 | 2.064 $\pm$ 0.004                 | 1.900 $\pm$ 0.002                 | 2.843 $\pm$ 0.003                 |
|                    | SPE           | 0.355 $\pm$ 0.001                 | 0.659 $\pm$ 0.002                 | 1.419 $\pm$ 0.013                 | 2.066 $\pm$ 0.005                 | 1.920 $\pm$ 0.000                 | 2.460 $\pm$ 0.008                 |
| SVD                | Naive         | 0.649 $\pm$ 0.002                 | 0.853 $\pm$ 0.002                 | 1.330 $\pm$ 0.003                 | 2.196 $\pm$ 0.002                 | 1.982 $\pm$ 0.004                 | 2.252 $\pm$ 0.007                 |
|                    | SignNet       | 0.673 $\pm$ 0.003                 | 0.872 $\pm$ 0.002                 | 1.564 $\pm$ 0.008                 | 2.229 $\pm$ 0.003                 | 1.996 $\pm$ 0.005                 | 2.520 $\pm$ 0.005                 |
|                    | SPE           | 0.727 $\pm$ 0.001                 | 0.912 $\pm$ 0.001                 | 2.176 $\pm$ 0.001                 | 2.261 $\pm$ 0.002                 | 2.122 $\pm$ 0.007                 | 2.969 $\pm$ 0.003                 |
| MagLap-1q (q=0.1)  | Naive         | 0.366 $\pm$ 0.003                 | 0.593 $\pm$ 0.003                 | 1.349 $\pm$ 0.040                 | 1.826 $\pm$ 0.005                 | 1.760 $\pm$ 0.007                 | 2.461 $\pm$ 0.008                 |
|                    | SignNet       | 0.554 $\pm$ 0.001                 | 0.699 $\pm$ 0.002                 | 1.721 $\pm$ 0.009                 | 2.048 $\pm$ 0.004                 | 1.881 $\pm$ 0.003                 | 2.726 $\pm$ 0.005                 |
|                    | SPE           | 0.124 $\pm$ 0.002                 | 0.433 $\pm$ 0.002                 | 0.584 $\pm$ 0.025                 | 1.620 $\pm$ 0.005                 | 1.547 $\pm$ 0.004                 | 1.302 $\pm$ 0.008                 |
| MagLap-1q (best q) | SPE           | 0.124 $\pm$ 0.002                 | 0.432 $\pm$ 0.004                 | 0.584 $\pm$ 0.025                 | 1.533 $\pm$ 0.007                 | 1.493 $\pm$ 0.003                 | 1.264 $\pm$ 0.020                 |
| MagLap-Multi-q     | Naive         | 0.353 $\pm$ 0.003                 | 0.535 $\pm$ 0.006                 | 1.196 $\pm$ 0.037                 | 1.708 $\pm$ 0.012                 | 1.661 $\pm$ 0.002                 | 2.055 $\pm$ 0.071                 |
|                    | SignNet       | 0.473 $\pm$ 0.000                 | 0.579 $\pm$ 0.001                 | 1.600 $\pm$ 0.039                 | 1.906 $\pm$ 0.001                 | 1.784 $\pm$ 0.008                 | 2.648 $\pm$ 0.013                 |
|                    | SPE           | <b>0.016<math>\pm</math>0.000</b> | <b>0.185<math>\pm</math>0.036</b> | <b>0.430<math>\pm</math>0.052</b> | <b>0.546<math>\pm</math>0.068</b> | <b>1.100<math>\pm</math>0.007</b> | <b>0.598<math>\pm</math>0.004</b> |

Note that in practice, if the backbone model is a GNN, only a portion of (sparse) entries  $[z_{\text{edge}}]_{u,v}$ ,  $(u, v) \in \mathcal{E}$  need to be computed. For the multi- $q$  case, we apply the same  $\phi_\ell$  and  $\rho$  to the eigenvectors and eigenvalues from different  $q$ 's and concatenate the outputs. A similar proof technique can show that the above stable PE framework can achieve generalization benefits as stated in Proposition 3.1 in [27]. Moreover, it can be shown that  $z_{\text{node}}$ ,  $z_{\text{edge}}$  are continuous in the choice of  $q$  due to the stable structure. Such continuity naturally unifies Lap-PE and Mag-PE, because symmetrized Laplacian  $L_s$  is a special case of Magnetic Laplacian  $L_q$  when  $q \rightarrow 0$ .

## 5 Experiments

In this section, we evaluate the effectiveness of multi- $q$  Mag-PEs by studying the following questions:

- **Q1:** How good are the previous PEs and our proposed PEs at expressing directed distances/relations, e.g., directed shortest/longest path distances and the walk profile?
- **Q2:** How do these PE methods perform on practical tasks and real-world datasets?
- **Q3:** What is the impact of using PEs with or without basis-invariant/stable architectures?

In our experiments, we mainly consider three ways of processing PEs: (1) Naïve: directly concatenates raw PEs with node features; (2) SignNet [37]: makes PEs sign invariant. We adopt the same pipeline as in [25], Figure G.1; (3) SPE (Eqs. (5),(6)): we follow [27], and use element-wise MLPs as  $\phi_1, \dots, \phi_m$ , GIN [60] as  $\rho_{\text{node}}$  and MLPs as  $\rho_{\text{edge}}$ . Key hyperparameters are included in the main text while full details of the experiment setup and model configurations can be found in Appendix B.

### 5.1 Distance Prediction on Directed Graphs

**Datasets.** To answer question **Q1**, we follow [25] and generate Erdős–Rényi random graphs. Specifically, we sample regular directed graphs with average node degree drawn from  $\{1, 1.5, 2\}$ , or directed acyclic graphs with average node degree from  $\{1, 1.5, 2, 2.5, 3\}$ . In both cases, there are 400,000 samples for training and validation (graph size from 16 to 63, training:validation=95:5), and 5,000 samples for test (graph size from 64 to 71). Finally, We take the largest connected component of each generated graph and form our final dataset. The task is to predict the pair-wise distances for node pairs measured by: (1) shortest path distance; (2) longest path distance; (3) walk profile. For the walk profile, we choose to predict the profile of length 4, which is a 5-dim vector. Only node pairs that are reachable or have non-zero walk profile elements are included for training and test.

**Models.** To show the power of pure PEs, we take PEs  $z_u, z_v$  of node  $u, v$  to predict the distance  $d_{u,v}$  between  $u, v$ . We consider three ways of processing PEs: (1) naïve concatenation:  $\text{MLP}([z_u, z_v])$ ; (2) SignNet-based:  $\text{MLP}(\text{SignNet}(z_u), \text{SignNet}(z_v))$ ; (3) edge-SPE-based:  $\text{MLP}([z_{\text{edge}}]_{u,v})$  where  $z_{\text{edge}}$  is defined in Eq. (6). For Multi- $q$  Magnetic Laplacian PE, we choose  $\vec{q} = (0, \frac{1}{2L}, \dots, \frac{L-1}{2L})$  where  $L = 5$  for predicting walk profile,  $L = 10$  for predicting shortest/longest path distances on directed acyclic graphs and  $L = 15$  for predicting shortest/longest path distances on regular directed graphs. For single- $q$  Mag-PE, we tune  $q$  from 0 to 0.5, and we report both the result of  $q = 0.1$  and the tuned best  $q$ . It turns out the performance of single- $q$  Mag-PE is not very sensitive to the value of  $q$  as long as it is not too large.

| PE method          | PE processing | Test F1                          |
|--------------------|---------------|----------------------------------|
| Lap                | Naive         | 51.39 $\pm$ 2.36                 |
|                    | SignNet       | 49.50 $\pm$ 4.01                 |
|                    | SPE           | 56.35 $\pm$ 3.70                 |
| Maglap-1q (best q) | Naive         | 68.68 $\pm$ 9.66                 |
|                    | SignNet       | 76.28 $\pm$ 6.82                 |
|                    | SPE           | 86.86 $\pm$ 3.85                 |
| Maglap-5q          | Naive         | 75.12 $\pm$ 12.78                |
|                    | SignNet       | 72.97 $\pm$ 9.38                 |
|                    | SPE           | <b>91.27<math>\pm</math>0.71</b> |

Table 2: Test F1 scores over 5 random seeds for sorting network satisfiability.

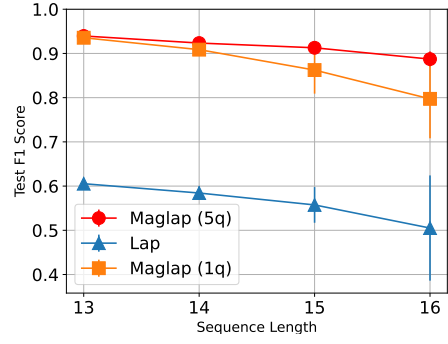


Figure 3: Test F1 scores w.r.t. different sorting network lengths.

**Results.** We have several observations from Table 1. (1) Multi-q Mag-PE constantly outperforms other PE methods regardless of how we process the PE. Particularly, it is significantly better than other methods when equipped with SPE, for instance, Multi-q Mag-PE with SPE gets test RMSE reduced by 53% on average compared to single-q Mag-PE with SPE. (2) *impact of symmetry*: when restricted to the use of naïve concatenation, the overall performance of all PE methods is not desired. This is because naïve concatenation cannot handle the basis ambiguity of eigenvectors. It is worth noticing that SignNet’s performance may be even worse than naïve concatenation. This makes sense because the PE processed by SignNet suffers from node ambiguity, which loses pair-wise distance information [36, 64]. Besides, SignNet is not stable, which could lead to a poor generalization error. In contrast, when we properly handle the complex eigenvectors by SPE, the true benefit of Mag-PE starts to present. On average the test RMSE of Multi-q Magnetic Laplacian gets reduced by 66% compared to naïve concatenation.

**Ablation study.** The comparison to single-q Mag-PE naturally serves as an ablation study of Multi-q Mag-PE. One may also wonder if Multi-q Mag-PE performs better simply because it can search and find the best  $q$  from  $\vec{q}$ . We can show that the joint use of different  $q$ ’s is indeed necessary, and it is constantly better than using a single best  $q$ . To show this, in all of the experiments we always conduct a hyper-parameter search over  $q$  for single-q Magnetic Laplacian and compare it with Multi-q Magnetic Laplacian. The results of tuning single  $q$  for different tasks can be found in Appendix C.

## 5.2 Sorting Network Satisfiability

Sorting network [30] is a comparison-based algorithm designed to perform sorting on a fixed number of variables. Each sorting network consists of a sequence of operations  $v_i, v_j = \text{sorted}(v_i, v_j)$  and we say a sorting network is satisfiable if it can correctly sort an arbitrary input of a given length. It can be parsed into a directed graph for which the direction (i.e., the order of operations) impacts the satisfiability. We test the ability of positional encodings by how well they can predict the satisfiability.

**Datasets.** We randomly generate sorting networks by following the setup from [25]. Sorting networks are parsed into directed acyclic graphs whose nodes are comparison operators and directed edges connect two operators that share variables to sort. The dataset contains 800,000 training samples with a length (the number of variables to sort) from 7 to 11, 60,000 validation samples with a length 12, and 60,000 test samples with a length from 13 to 16. We perform graph classification to predict satisfiability.

**Models.** We adopt a vanilla transformer [53] as our base model. PEs are either naively concatenated into node features, or using SignNet before concatenation, or concatenated both into node features and attention weights using SPEs Eqs.(5) and (6). For single-q Magnetic Laplacian PE, we tune  $q$  from  $\frac{1}{20 \cdot d_G}$  to  $\frac{5}{20 \cdot d_G}$ , where  $d_G = \max(\min(m, n), 1)$ ,  $m$  is the number of directed edges and  $n$  is the number of nodes. We find  $q = \frac{5}{20 \cdot d_G}$  gives the best results, which is the same  $q$  as in [25]. For multi-q Mag-PE, we choose  $\vec{q} = (\frac{1}{20 \cdot d_G}, \dots, \frac{5}{20 \cdot d_G})$ .

**Results.** Table 2 displays the average Test F1 score of classifying satisfiability. Again, Multi-q Mag-PE equipped with SPE achieves the best performance. Mag-PE with SignNet (both single-q and



Table 3: Test results (RMSE for Gain/BW/PM, MSE for DSP/LUT) for circuit properties prediction. **Bold** denotes the best result for each base model, and **Bold<sup>†</sup>** for the best result among all base models.

| Base Model           | PE method          | PE processing | Gain                              | BW                                | PM                                | DSP                               | LUT                               |
|----------------------|--------------------|---------------|-----------------------------------|-----------------------------------|-----------------------------------|-----------------------------------|-----------------------------------|
| Undirected-GIN       | Lap                | SignNet       | 0.430 $\pm$ 0.009                 | 4.712 $\pm$ 0.134                 | 1.127 $\pm$ 0.007                 | 2.665 $\pm$ 0.184                 | 2.025 $\pm$ 0.057                 |
|                      |                    | SPE           | 0.416 $\pm$ 0.021                 | 4.321 $\pm$ 0.084                 | 1.127 $\pm$ 0.020                 | 2.662 $\pm$ 0.187                 | <b>1.925<math>\pm</math>0.059</b> |
|                      | Maglap-1q (q=0.01) | SignNet       | 0.426 $\pm$ 0.009                 | 4.670 $\pm$ 0.113                 | 1.116 $\pm$ 0.009                 | 2.673 $\pm$ 0.090                 | 2.027 $\pm$ 0.091                 |
|                      |                    | SPE           | 0.405 $\pm$ 0.016                 | 4.305 $\pm$ 0.092                 | 1.121 $\pm$ 0.018                 | 2.666 $\pm$ 0.190                 | 2.024 $\pm$ 0.068                 |
|                      | Maglap-1q (best q) | SPE           | 0.398 $\pm$ 0.025                 | 4.281 $\pm$ 0.085                 | <b>1.113<math>\pm</math>0.022</b> | 2.614 $\pm$ 0.098                 | 2.010 $\pm$ 0.082                 |
|                      | Maglap-Multi-q     | SignNet       | 0.421 $\pm$ 0.015                 | 4.743 $\pm$ 0.215                 | 1.126 $\pm$ 0.011                 | 2.665 $\pm$ 0.111                 | 2.025 $\pm$ 0.076                 |
|                      |                    | SPE           | <b>0.389<math>\pm</math>0.017</b> | <b>4.175<math>\pm</math>0.115</b> | 1.137 $\pm$ 0.004                 | <b>2.582<math>\pm</math>0.133</b> | 1.976 $\pm$ 0.089                 |
| Bidirected-GIN       | Lap                | SignNet       | 0.382 $\pm$ 0.008                 | 4.371 $\pm$ 0.171                 | 1.127 $\pm$ 0.021                 | 2.256 $\pm$ 0.109                 | 1.806 $\pm$ 0.096                 |
|                      |                    | SPE           | 0.391 $\pm$ 0.007                 | 4.153 $\pm$ 0.160                 | 1.135 $\pm$ 0.035                 | 2.267 $\pm$ 0.126                 | 1.786 $\pm$ 0.072                 |
|                      | Maglap-1q (q=0.01) | SignNet       | 0.388 $\pm$ 0.012                 | 4.351 $\pm$ 0.132                 | 1.131 $\pm$ 0.012                 | 2.304 $\pm$ 0.143                 | 1.882 $\pm$ 0.085                 |
|                      |                    | SPE           | 0.384 $\pm$ 0.008                 | 4.152 $\pm$ 0.056                 | 1.123 $\pm$ 0.026                 | 2.344 $\pm$ 0.134                 | 1.830 $\pm$ 0.116                 |
|                      | Maglap-1q (best q) | SPE           | 0.383 $\pm$ 0.002                 | 4.113 $\pm$ 0.052                 | <b>1.099<math>\pm</math>0.020</b> | 2.256 $\pm$ 0.144                 | 1.768 $\pm$ 0.090                 |
|                      | Maglap-Multi-q     | SignNet       | 0.381 $\pm$ 0.008                 | 4.443 $\pm$ 0.116                 | 1.119 $\pm$ 0.016                 | 2.212 $\pm$ 0.116                 | 1.791 $\pm$ 0.091                 |
|                      |                    | SPE           | <b>0.371<math>\pm</math>0.008</b> | <b>4.051<math>\pm</math>0.139</b> | 1.116 $\pm$ 0.012                 | <b>2.207<math>\pm</math>0.185</b> | <b>1.735<math>\pm</math>0.096</b> |
| SAT (undirected-GIN) | Lap                | SignNet       | 0.368 $\pm$ 0.022                 | 4.085 $\pm$ 0.189                 | 1.038 $\pm$ 0.016                 | 3.103 $\pm$ 0.101                 | 2.223 $\pm$ 0.175                 |
|                      |                    | SPE           | 0.375 $\pm$ 0.016                 | 4.180 $\pm$ 0.093                 | 1.065 $\pm$ 0.034                 | 3.167 $\pm$ 0.193                 | 2.425 $\pm$ 0.168                 |
|                      | Maglap-1q (q=0.01) | SignNet       | 0.382 $\pm$ 0.009                 | 4.143 $\pm$ 0.181                 | 1.073 $\pm$ 0.021                 | 3.087 $\pm$ 0.183                 | 2.214 $\pm$ 0.150                 |
|                      |                    | SPE           | 0.366 $\pm$ 0.003                 | 4.081 $\pm$ 0.071                 | 1.089 $\pm$ 0.023                 | 3.206 $\pm$ 0.197                 | 2.362 $\pm$ 0.154                 |
|                      | Maglap-1q (best q) | SPE           | 0.361 $\pm$ 0.016                 | <b>4.014<math>\pm</math>0.068</b> | 1.057 $\pm$ 0.036                 | 3.101 $\pm$ 0.176                 | 2.362 $\pm$ 0.154                 |
|                      | Maglap-Multi-q     | SignNet       | 0.368 $\pm$ 0.020                 | 4.044 $\pm$ 0.090                 | 1.066 $\pm$ 0.028                 | 3.121 $\pm$ 0.143                 | <b>2.207<math>\pm</math>0.113</b> |
|                      |                    | SPE           | <b>0.350<math>\pm</math>0.004</b> | 4.044 $\pm$ 0.153                 | <b>1.035<math>\pm</math>0.025</b> | <b>3.076<math>\pm</math>0.240</b> | 2.333 $\pm$ 0.147                 |
| SAT (bidirected-GIN) | Lap                | SignNet       | 0.384 $\pm$ 0.025                 | 3.949 $\pm$ 0.125                 | 1.069 $\pm$ 0.029                 | <b>2.569<math>\pm</math>0.116</b> | 2.048 $\pm$ 0.088                 |
|                      |                    | SPE           | 0.368 $\pm$ 0.022                 | 4.024 $\pm$ 0.106                 | <b>1.044<math>\pm</math>0.021</b> | 2.713 $\pm$ 0.135                 | 2.173 $\pm$ 0.107                 |
|                      | Maglap-1q (q=0.01) | SignNet       | 0.384 $\pm$ 0.015                 | 4.023 $\pm$ 0.032                 | 1.055 $\pm$ 0.028                 | 2.616 $\pm$ 0.120                 | 2.054 $\pm$ 0.127                 |
|                      |                    | SPE           | 0.364 $\pm$ 0.012                 | 3.996 $\pm$ 0.178                 | 1.074 $\pm$ 0.030                 | 2.687 $\pm$ 0.209                 | 2.192 $\pm$ 0.135                 |
|                      | Maglap-1q (best q) | SPE           | <b>0.360<math>\pm</math>0.009</b> | 3.960 $\pm$ 0.060                 | 1.062 $\pm$ 0.024                 | 2.657 $\pm$ 0.128                 | 2.107 $\pm$ 0.135                 |
|                      | Maglap-Multi-q     | SignNet       | 0.420 $\pm$ 0.035                 | 4.022 $\pm$ 0.128                 | 1.089 $\pm$ 0.046                 | 2.741 $\pm$ 0.110                 | <b>2.045<math>\pm</math>0.079</b> |
|                      |                    | SPE           | <b>0.359<math>\pm</math>0.008</b> | <b>3.930<math>\pm</math>0.069</b> | <b>1.045<math>\pm</math>0.012</b> | 2.616 $\pm$ 0.151                 | 2.082 $\pm$ 0.099                 |

multi-q) performs poorly compared to their SPE counterparts. Figure 3 additionally illustrates the test F1 on samples with respect to individual sorting network lengths. Note that although single-q Mag-PE and multi-q Mag-PE perform equally well on length=13 samples, the single-q one generalizes worse on longer-length sorting networks. In contrast, Multi-q Mag-PE has nearly the same generalization performance as the number of variables to sort increases.

### 5.3 Circuit Property Prediction

We evaluate different PE methods on real-world Circuit Property Prediction tasks.

**Open Circuit Benchmark.** Open Circuit Benchmark [16] contains 10,000 operational amplifiers circuits as directed graphs and the task is to predict the DC gain (Gain), band width (BW) and phase margin (PM) of each circuit. These targets reflect the property of current flows from input nodes to output nodes and thus require a powerful direction-aware model. The dataset consists of 2-stage amplifiers and 3-stage amplifiers and we use 2-stage amplifiers in our experiment. We randomly split them into 0.9:0.05:0.05 as training, validation and test set.

**High-level Synthesis.** The HLS dataset [58] collects 18,750 intermediate representation (IR) graphs of C/C++ code after front-end compilation [3]. It provides post-implementation performance metrics on FPGA devices as labels, which are obtained after hours of synthesis using the Vitis HLS tool [1] and implementation with Vivado [2]. The task is to predict resource usage, namely look-up table (LUT) and digital signal processor (DSP) usage. We randomly select 16570 for training, and 1000 each for validation and testing.

**Models.** We adopt GIN [60] as the backbone and implement two variants: (1) undirected-GIN: the normal GIN works on the undirected version of the original directed graphs; (2) bidirectional-GIN: bidirectional message passing with different weights for two directions, inspired by [29, 50, 57]. The state-of-the-art graph transformer SAT [10] is also adopted, whose GNN extractor is undirected-GIN or bidirected-GIN as mentioned for self-attention computation. PEs are processed and then concatenated with node features using SignNet or with node and edge features using SPE (Eqs. (5), (6)). We generally choose  $\vec{q} = (1, 2, \dots, 10)/100$  or  $\vec{q} = (1, 2, \dots, 5)/100$  for Multi-q Mag-PE (see Appendix B for specific  $q$  for each tasks). For single-q Magnetic Laplacian, we report  $q = 0.01$  as well as the best results of single  $q$  by searching over the range of multiple  $q$ . See Appendix C for full results of varying single  $q$ .

**Results.** Table 3 shows the test RMSE (5 random seeds) on Open Circuit Benchmark (Gain, BW, PM) and the test MSE (10 random seeds) on high-level synthesis (DSP, LUT). Notably, Multi-q Mag-PE with Stable PE framework achieves the best results for all 5 targets.

## 6 Conclusion and Limitations

We study the positional encodings (PEs) for directed graphs. We propose the notion of walk profile to assess the model’s ability to encode directed relation. Limitations of existing PEs to express walk profiles are identified. We propose a simple yet effective variant of Magnetic Laplacian PE called Multi-q Mag-PE that can provably compute walk profile. Finally, we extend the previous basis-invariant and stable PE framework and address the basis ambiguity and stability problem of complex eigenvectors. Experiments demonstrate the consistent performance gain of Multi-q Mag-PE.

One limitation of our work is the overhead of computing and storing multiple eigendecompositions. One possible way to alleviate this is to randomly sample certain number of potential factors to make computation affordable, which can be a future work.

## Acknowledgments

This research is supported by the NSF awards IIS-2239565.

## References

- [1] Vitis hls tool. <https://www.xilinx.com/products/design-tools/vitis/vitis-hls.html>.
- [2] Vivado. <https://www.xilinx.com/products/design-tools/vivado.html>.
- [3] V Aho Alfred, S Lam Monica, and D Ullman Jeffrey. *Compilers Principles, Techniques & Tools*. pearson Education, 2007.
- [4] Miltiadis Allamanis. Graph neural networks in program analysis. *Graph neural networks: foundations, frontiers, and applications*, pages 483–497, 2022.
- [5] Dominique Beaini, Saro Passaro, Vincent Létourneau, Will Hamilton, Gabriele Corso, and Pietro Liò. Directional graph networks. In *International Conference on Machine Learning*, pages 748–758. PMLR, 2021.
- [6] Mitchell Black, Zhengchao Wan, Gal Mishne, Amir Nayyeri, and Yusu Wang. Comparing graph transformers via positional encodings. *arXiv preprint arXiv:2402.14202*, 2024.
- [7] Vladimir Boginski, Sergiy Butenko, and Panos M Pardalos. Statistical analysis of financial networks. *Computational statistics & data analysis*, 48(2):431–443, 2005.
- [8] Alexander Brauckmann, Andrés Goens, Sebastian Ertel, and Jeronimo Castrillon. Compiler-based graph representations for deep learning models of code. In *Proceedings of the 29th International Conference on Compiler Construction*, pages 201–211, 2020.
- [9] Michael M Bronstein, Joan Bruna, Yann LeCun, Arthur Szlam, and Pierre Vandergheynst. Geometric deep learning: going beyond euclidean data. *IEEE Signal Processing Magazine*, 34(4):18–42, 2017.
- [10] Dexiong Chen, Leslie O’Bray, and Karsten Borgwardt. Structure-aware transformer for graph representation learning. In *International Conference on Machine Learning*, pages 3469–3489. PMLR, 2022.
- [11] H-C Chen and DH-C Du. Path sensitization in critical path problem (logic circuit design). *IEEE Transactions on Computer-Aided Design of Integrated Circuits and Systems*, 12(2):196–207, 1993.
- [12] Fan RK Chung. *Spectral graph theory*, volume 92. American Mathematical Soc., 1997.
- [13] RR Coifman and S Lafon. Diffusion maps: Applied and computational harmonic analysis. *Appl Comput Harmon Anal*, 21(1):5–14, 2004.
- [14] Chris Cummins, Zacharias V Fisches, Tal Ben-Nun, Torsten Hoefer, Michael FP O’Boyle, and Hugh Leather. Programl: A graph-based program representation for data flow analysis and compiler optimizations. In *International Conference on Machine Learning*, pages 2244–2253. PMLR, 2021.
- [15] Chris Cummins, Hugh Leather, Zacharias Fisches, Tal Ben-Nun, Torsten Hoefer, and Michael O’Boyle. Deep data flow analysis. *arXiv preprint arXiv:2012.01470*, 2020.
- [16] Zehao Dong, Weidong Cao, Muhan Zhang, Dacheng Tao, Yixin Chen, and Xuan Zhang. Cktgnn: Circuit graph neural network for electronic design automation. In *The Eleventh International Conference on Learning Representations*, 2022.
- [17] Zehao Dong, Muhan Zhang, Fuhai Li, and Yixin Chen. Pace: A parallelizable computation encoder for directed acyclic graphs. In *International Conference on Machine Learning*, pages 5360–5377. PMLR, 2022.
- [18] Alexey Dosovitskiy, Lucas Beyer, Alexander Kolesnikov, Dirk Weissenborn, Xiaohua Zhai, Thomas Unterthiner, Mostafa Dehghani, Matthias Minderer, Georg Heigold, Sylvain Gelly, et al. An image is worth 16x16 words: Transformers for image recognition at scale. In *International Conference on Learning Representations*, 2020.

- [19] Vijay Prakash Dwivedi, Chaitanya K. Joshi, Anh Tuan Luu, Thomas Laurent, Yoshua Bengio, and Xavier Bresson. Benchmarking graph neural networks. *Journal of Machine Learning Research*, 24(43):1–48, 2023.
- [20] Vijay Prakash Dwivedi, Anh Tuan Luu, Thomas Laurent, Yoshua Bengio, and Xavier Bresson. Graph neural networks with learnable structural and positional representations. In *International Conference on Learning Representations*, 2021.
- [21] Michaël Fanuel, Carlos M Alaíz, Ángela Fernández, and Johan AK Suykens. Magnetic eigenmaps for the visualization of directed networks. *Applied and Computational Harmonic Analysis*, 44(1):189–199, 2018.
- [22] Michaël Fanuel, Carlos M Alaiz, and Johan AK Suykens. Magnetic eigenmaps for community detection in directed networks. *Physical Review E*, 95(2):022302, 2017.
- [23] Stefano Fiorini, Stefano Coniglio, Michele Ciavotta, and Enza Messina. Sigmanet: One laplacian to rule them all. In *Proceedings of the AAAI Conference on Artificial Intelligence*, volume 37, pages 7568–7576, 2023.
- [24] Satoshi Furutani, Toshiki Shibahara, Mitsuaki Akiyama, Kunio Hato, and Masaki Aida. Graph signal processing for directed graphs based on the hermitian laplacian. In *Machine Learning and Knowledge Discovery in Databases: European Conference, ECML PKDD 2019, Würzburg, Germany, September 16–20, 2019, Proceedings, Part I*, pages 447–463. Springer, 2020.
- [25] Simon Geisler, Yujia Li, Daniel J Mankowitz, Ali Taylan Cemgil, Stephan Günnemann, and Cosmin Paduraru. Transformers meet directed graphs. In *International Conference on Machine Learning*, pages 11144–11172. PMLR, 2023.
- [26] Yixuan He, Michael Perlmutter, Gesine Reinert, and Mihai Cucuringu. Msgnn: A spectral graph neural network based on a novel magnetic signed laplacian. In *Learning on Graphs Conference*, pages 40–1. PMLR, 2022.
- [27] Yinan Huang, William Lu, Joshua Robinson, Yu Yang, Muhan Zhang, Stefanie Jegelka, and Pan Li. On the stability of expressive positional encodings for graph neural networks. *arXiv preprint arXiv:2310.02579*, 2023.
- [28] Md Shamim Hussain, Mohammed J Zaki, and Dharmashankar Subramanian. Global self-attention as a replacement for graph convolution. In *Proceedings of the 28th ACM SIGKDD Conference on Knowledge Discovery and Data Mining*, pages 655–665, 2022.
- [29] Guillaume Jaume, An-Phi Nguyen, Maria Rodriguez Martinez, Jean-Philippe Thiran, and Maria Gabrani. edggn: A simple and powerful gnn for directed labeled graphs. In *International Conference on Learning Representations*, 2019.
- [30] Donald Ervin Knuth. *The art of computer programming*, volume 3. Pearson Education, 1997.
- [31] Christian Koke and Daniel Cremers. Holonets: Spectral convolutions do extend to directed graphs. In *The Twelfth International Conference on Learning Representations*, 2023.
- [32] Georgios Kollias, Vasileios Kalantzis, Tsuyoshi Idé, Aurélie Lozano, and Naoki Abe. Directed graph auto-encoders. In *Proceedings of the AAAI conference on artificial intelligence*, volume 36, pages 7211–7219, 2022.
- [33] Devin Kreuzer, Dominique Beaini, Will Hamilton, Vincent Létourneau, and Prudencio Tossou. Rethinking graph transformers with spectral attention. *Advances in Neural Information Processing Systems*, 34, 2021.
- [34] Pan Li and Jure Leskovec. The expressive power of graph neural networks. *Graph Neural Networks: Foundations, Frontiers, and Applications*, pages 63–98, 2022.
- [35] Pan Li, Yanbang Wang, Hongwei Wang, and Jure Leskovec. Distance encoding: Design provably more powerful neural networks for graph representation learning. *Advances in Neural Information Processing Systems*, 33:4465–4478, 2020.

- [36] Derek Lim, Joshua Robinson, Stefanie Jegelka, and Haggai Maron. Expressive sign equivariant networks for spectral geometric learning. *Advances in Neural Information Processing Systems*, 36, 2023.
- [37] Derek Lim, Joshua Robinson, Lingxiao Zhao, Tess Smidt, Suvrit Sra, Haggai Maron, and Stefanie Jegelka. Sign and basis invariant networks for spectral graph representation learning. *arXiv preprint arXiv:2202.13013*, 2022.
- [38] Yaron Lipman, Raif M Rustamov, and Thomas A Funkhouser. Biharmonic distance. *ACM Transactions on Graphics (TOG)*, 29(3):1–11, 2010.
- [39] Hanwen Liu, Huaizhen Kou, Chao Yan, and Lianyong Qi. Link prediction in paper citation network to construct paper correlation graph. *EURASIP Journal on Wireless Communications and Networking*, 2019(1):1–12, 2019.
- [40] Yuankai Luo, Veronika Thost, and Lei Shi. Transformers over directed acyclic graphs. *Advances in Neural Information Processing Systems*, 36, 2024.
- [41] Yi Ma, Jianye Hao, Yaodong Yang, Han Li, Junqi Jin, and Guangyong Chen. Spectral-based graph convolutional network for directed graphs. *arXiv preprint arXiv:1907.08990*, 2019.
- [42] Federico Monti, Karl Otness, and Michael M Bronstein. Motifnet: a motif-based graph convolutional network for directed graphs. In *2018 IEEE data science workshop (DSW)*, pages 225–228. IEEE, 2018.
- [43] Mangpo Phothilimthana, Sami Abu-El-Haija, Kaidi Cao, Bahare Fatemi, Michael Burrows, Charith Mendis, and Bryan Perozzi. Tugraphs: A performance prediction dataset on large tensor computational graphs. *Advances in Neural Information Processing Systems*, 36, 2024.
- [44] Haiquan Qiu, Yongqi Zhang, Yong Li, and Quanming Yao. Logical expressiveness of graph neural network for knowledge graph reasoning. *arXiv preprint arXiv:2303.12306*, 2023.
- [45] Ladislav Rampásek, Michael Galkin, Vijay Prakash Dwivedi, Anh Tuan Luu, Guy Wolf, and Dominique Beaini. Recipe for a general, powerful, scalable graph transformer. *Advances in Neural Information Processing Systems*, 35:14501–14515, 2022.
- [46] Pengzhen Ren, Yun Xiao, Xiaojun Chang, Po-Yao Huang, Zhihui Li, Xiaojiang Chen, and Xin Wang. A comprehensive survey of neural architecture search: Challenges and solutions. *ACM Computing Surveys (CSUR)*, 54(4):1–34, 2021.
- [47] MA Shubin. Discrete magnetic laplacian. *Communications in mathematical physics*, 164(2):259–275, 1994.
- [48] Rahul Singh, Abhishek Chakraborty, and BS Manoj. Graph fourier transform based on directed laplacian. In *2016 International Conference on Signal Processing and Communications (SPCOM)*, pages 1–5. IEEE, 2016.
- [49] Jianlin Su, Murtadha Ahmed, Yu Lu, Shengfeng Pan, Wen Bo, and Yunfeng Liu. Roformer: Enhanced transformer with rotary position embedding. *Neurocomputing*, 568:127063, 2024.
- [50] Veronika Thost and Jie Chen. Directed acyclic graph neural networks. In *International Conference on Learning Representations*, 2020.
- [51] Ling Tian, Xue Zhou, Yan-Ping Wu, Wang-Tao Zhou, Jin-Hao Zhang, and Tian-Shu Zhang. Knowledge graph and knowledge reasoning: A systematic review. *Journal of Electronic Science and Technology*, 20(2):100159, 2022.
- [52] Zekun Tong, Yuxuan Liang, Changsheng Sun, David S Rosenblum, and Andrew Lim. Directed graph convolutional network. *arXiv preprint arXiv:2004.13970*, 2020.
- [53] Ashish Vaswani, Noam Shazeer, Niki Parmar, Jakob Uszkoreit, Llion Jones, Aidan N Gomez, Łukasz Kaiser, and Illia Polosukhin. Attention is all you need. *Advances in neural information processing systems*, 30, 2017.

- [54] Hanrui Wang, Kuan Wang, Jiacheng Yang, Linxiao Shen, Nan Sun, Hae-Seung Lee, and Song Han. Gcn-rl circuit designer: Transferable transistor sizing with graph neural networks and reinforcement learning. In *2020 57th ACM/IEEE Design Automation Conference (DAC)*, pages 1–6. IEEE, 2020.
- [55] Haorui Wang, Haoteng Yin, Muhan Zhang, and Pan Li. Equivariant and stable positional encoding for more powerful graph neural networks. *arXiv preprint arXiv:2203.00199*, 2022.
- [56] Xiyuan Wang, Pan Li, and Muhan Zhang. Graph as point set. *arXiv preprint arXiv:2405.02795*, 2024.
- [57] Wei Wen, Hanxiao Liu, Yiran Chen, Hai Li, Gabriel Bender, and Pieter-Jan Kindermans. Neural predictor for neural architecture search. In *European conference on computer vision*, pages 660–676. Springer, 2020.
- [58] Nan Wu, Hang Yang, Yuan Xie, Pan Li, and Cong Hao. High-level synthesis performance prediction using gnns: Benchmarking, modeling, and advancing. In *Proceedings of the 59th ACM/IEEE Design Automation Conference*, pages 49–54, 2022.
- [59] Wenjun Xiao and Ivan Gutman. Resistance distance and laplacian spectrum. *Theoretical chemistry accounts*, 110:284–289, 2003.
- [60] Keyulu Xu, Weihua Hu, Jure Leskovec, and Stefanie Jegelka. How powerful are graph neural networks? In *International Conference on Learning Representations*, 2018.
- [61] Chulhee Yun, Srinadh Bhojanapalli, Ankit Singh Rawat, Sashank Reddi, and Sanjiv Kumar. Are transformers universal approximators of sequence-to-sequence functions? In *International Conference on Learning Representations*, 2019.
- [62] Guo Zhang, Hao He, and Dina Katabi. Circuit-gnn: Graph neural networks for distributed circuit design. In *International conference on machine learning*, pages 7364–7373. PMLR, 2019.
- [63] Muhan Zhang, Shali Jiang, Zhicheng Cui, Roman Garnett, and Yixin Chen. D-vae: A variational autoencoder for directed acyclic graphs. *Advances in neural information processing systems*, 32, 2019.
- [64] Muhan Zhang, Pan Li, Yinglong Xia, Kai Wang, and Long Jin. Labeling trick: A theory of using graph neural networks for multi-node representation learning. *Advances in Neural Information Processing Systems*, 34:9061–9073, 2021.
- [65] Xitong Zhang, Yixuan He, Nathan Brugnone, Michael Perlmutter, and Matthew Hirn. Magnet: A neural network for directed graphs. *Advances in neural information processing systems*, 34:27003–27015, 2021.
- [66] Yaqin Zhou, Shangqing Liu, Jingkai Siow, Xiaoning Du, and Yang Liu. Devign: Effective vulnerability identification by learning comprehensive program semantics via graph neural networks. *Advances in neural information processing systems*, 32, 2019.

## A Deferred Proofs

### A.1 Proof of Theorem 4.1

**Theorem 4.1.** Fix a  $q \in \mathbb{R}$ . There exist graphs  $\mathcal{G}, \mathcal{G}'$  with adjacency matrices  $\mathbf{A}, \mathbf{A}' \in \mathbb{C}^{n \times n}$ , and nodes  $u, v \in V_{\mathcal{G}}$  and  $u', v' \in V_{\mathcal{G}'}$ , such that  $\text{Mag-PE}(\lambda, z_u, z_v) = (\lambda', z'_{u'}, z'_{v'})$ , but  $\Phi_{u,v}(m, k) \neq \Phi'_{u',v'}(m, k)$  for some  $m, k$ .

*Proof.* Proof by construction. Fix a  $q \in \mathbb{R}$ . Let  $\mathbf{A} \in \mathbb{C}^{n \times n}$  be any adjacency matrix with complex weight such that there is at most one directed edge between any node pairs  $u, v$ , i.e.,  $\mathbf{A}_{u,v}$  and  $\mathbf{A}_{v,u}$  cannot be both nonzero. Now, define  $\mathbf{A}'$  in the following way:

$$\mathbf{A}'_{u,v} = |\mathbf{A}_{v,u}| \exp\{-i(\angle \mathbf{A}_{v,u} + 4\pi q)\} \quad (7)$$

for all  $u, v$ , where  $|\mathbf{A}_{v,u}|, \angle \mathbf{A}_{v,u}$  are the amplitude and phase of complex number  $\mathbf{A}_{v,u}$  respectively. Note that  $\mathbf{A}'$  corresponds to a reverse version of original graph  $\mathbf{A}$ . Magnetic Laplacian of complex adjacency matrix is defined by  $\mathbf{L}_q = \mathbf{I} - \mathbf{D}^{-1/2} \mathbf{A}_q \mathbf{D}^{-1/2}$  and

$$[\mathbf{A}_q]_{u,v} = \begin{cases} \mathbf{A}_{u,v} \exp\{i2\pi q\}, & \text{if } (u, v) \in \mathcal{E}, \\ \mathbf{A}_{v,u}^* \exp\{-i2\pi q\}, & \text{if } (v, u) \in \mathcal{E}. \end{cases} \quad (8)$$

Now consider the Magnetic Laplacian induced by  $\mathbf{A}'$ . For  $(v, u) \in \mathcal{E}$ , we have

$$\begin{aligned} [\mathbf{A}'_q]_{u,v} &= \mathbf{A}'_{u,v} \exp\{i2\pi q\} = |\mathbf{A}_{v,u}| \exp\{-i(\angle \mathbf{A}_{v,u} + 4\pi q)\} \exp\{i2\pi q\} \\ &= \mathbf{A}_{v,u}^* \exp\{-i2\pi q\} = [\mathbf{A}_q]_{u,v}. \end{aligned} \quad (9)$$

Due to Hermitian property of  $\mathbf{A}_q, \mathbf{A}'_q$ , we can say  $\mathbf{A}_q = \mathbf{A}'_q$  for all  $u, v$ . As a result,  $\mathbf{L}_q = \mathbf{L}'_q$ , and thus resulting eigenvectors and eigenvalues are the same. On the other hand,  $\Phi_{u,v}$  and  $\Phi'_{u,v}$  are clearly different. For example,  $\Phi_{u,v}(1, 1) = [\mathbf{A}]_{u,v} \neq [\mathbf{A}']_{u,v} = \Phi'_{u,v}(1, 1)$ .  $\square$

### A.2 Proof of Theorem 4.2

**Theorem 4.2.** Let  $L$  be a positive integer. If we let  $\vec{q} = (q_1, q_2, \dots, q_{L+1})$  with  $L+1$  distinct  $q$ 's and  $q_1, \dots, q_{L+1} \in [0, \frac{1}{2})$ , then for all  $\ell \leq L$  and  $k \leq \ell$ , walk profile  $\Phi_{u,v}(\ell, k)$  can be computed from  $(\lambda^{\vec{q}}, z_u^{\vec{q}}, z_v^{\vec{q}})$ , where  $\lambda^{\vec{q}}, z^{\vec{q}}$  are concatenation of eigenvalues/eigenvectors of different  $q$  from  $\vec{q}$ .

*Proof.* The proof starts with identifying a key relation between  $[\mathbf{A}_q]_{u,v}^\ell$  and  $\Phi_{u,v}^\ell$ . Note that  $[\mathbf{A}_q]_{u,v}^\ell$  equals to the sum of weight of all length- $\ell$  bidirectional walks:

$$\begin{aligned} [\mathbf{A}_q]_{u,v}^\ell &= \sum_{w_1, w_2, \dots, w_{\ell-1}} [\mathbf{A}_q]_{u, w_1} [\mathbf{A}_q]_{w_1, w_2} \dots [\mathbf{A}_q]_{w_{\ell-1}, v} \\ &= \sum_{\substack{\text{bi-walk } (u, w_1, \dots, w_{\ell-1}, v) \\ \text{of length } \ell}} [\mathbf{A}_q]_{u, w_1} [\mathbf{A}_q]_{w_1, w_2} \dots [\mathbf{A}_q]_{w_{\ell-1}, v}. \end{aligned} \quad (10)$$

It is bidirectional because  $\mathbf{A}_q$  is Hermitian and allows transition along the forward edges with weight  $\mathbf{A}_{u,v} \exp\{i2\pi q\}$  or backward edges with weight  $\mathbf{A}_{u,v}^* \exp\{-i2\pi q\}$ . Note that we can categorize the bidirectional walks by their number of forward and reverse edges. For bidirectional walk of length  $\ell$  and exact  $k$  forward edges, the forward edges will cause an additional phase term  $\exp\{i2\pi k\}$  while the remaining  $\ell - k$  backward edges will cause  $\exp\{-i2\pi(\ell - k)\} = \exp\{i2\pi(k - \ell)\}$ . So there is a common phase term  $\exp\{i2\pi(2k - \ell)\}$  for all bidirectional walks of length  $\ell$  and  $k$  forward edges. Now we can re-organize the formula into

$$\begin{aligned} [\mathbf{A}_q]_{u,v}^\ell &= \sum_{k=0}^{\ell} \sum_{\substack{\text{bi-walk } (u, w_1, \dots, w_{\ell-1}, v) \\ \text{of length } \ell \text{ and } k \text{ forward edges}}} [\mathbf{A}_q]_{u, w_1} [\mathbf{A}_q]_{w_1, w_2} \dots [\mathbf{A}_q]_{w_{\ell-1}, v} \\ &= \sum_{k=0}^{\ell} \sum_{\substack{\text{bi-walk } (u, w_1, \dots, w_{\ell-1}, v) \\ \text{of length } \ell \text{ and } k \text{ forward edges}}} \exp\{i2\pi(2k - \ell)\} [\mathbf{A}_1]_{u, w_1} [\mathbf{A}_2]_{w_1, w_2} \dots [\mathbf{A}_\ell]_{w_{\ell-1}, v}, \end{aligned} \quad (11)$$

where  $\mathbf{A}_1, \dots, \mathbf{A}_\ell$  is either  $\mathbf{A}$  or  $\mathbf{A}^\dagger$ , depending on it is a forward or backward edge. Now by taking phase term  $\exp\{2i\pi(2k - \ell)\}$  out the inner sum, we get exactly walk profile:

$$\begin{aligned}
[\mathbf{A}_q]_{u,v}^\ell &= \sum_{k=0}^{\ell} \exp\{i2\pi(2k - \ell)\} \sum_{\substack{\text{bi-walk}(u, w_1, \dots, w_{\ell-1}, v) \\ \text{of length } \ell \text{ and } k \text{ forward edges}}} [\mathbf{A}_1]_{u, w_1} [\mathbf{A}_2]_{w_1, w_2} \dots [\mathbf{A}_\ell]_{w_{\ell-1}, v} \\
&= \sum_{k=0}^{\ell} \exp\{i2\pi(2k - \ell)\} \sum_{\substack{\mathbf{A}_i \in \{\mathbf{A}, \mathbf{A}^\top\} \\ k \text{ of } \mathbf{A}_1, \dots, \mathbf{A}_\ell \text{ is } \mathbf{A}}} [\mathbf{A}_1 \mathbf{A}_2 \dots \mathbf{A}_\ell]_{u,v} \\
&= \sum_{k=0}^{\ell} \exp\{i2\pi(2k - \ell)\} \Phi_{u,v}(\ell, k) \\
&= \exp\{-i2\pi\ell\} \sum_{k=0}^{\ell} \exp\{i4\pi k\} \Phi_{u,v}(\ell, k).
\end{aligned} \tag{12}$$

Let  $L$  be any positive integer. Let us write the relation above for  $\Phi_{u,v}(\ell, \cdot)$  ( $\ell \leq L$ ) in a matrix form:

$$\mathbf{F}_q \begin{pmatrix} \Phi_{u,v}(1, 0) & \Phi_{u,v}(2, 0) & \dots & \Phi_{u,v}(L, 0) \\ \Phi_{u,v}(1, 1) & \Phi_{u,v}(2, 1) & \dots & \Phi_{u,v}(L, 1) \\ 0 & \Phi_{u,v}(2, 2) & \dots & \Phi_{u,v}(L, 2) \\ 0 & 0 & \dots & \Phi_{u,v}(L, 3) \\ \dots & \dots & \dots & \Phi_{u,v}(L, L) \end{pmatrix} = \begin{pmatrix} e^{i2\pi} [\mathbf{A}_q]_{u,v} & e^{i4\pi} [\mathbf{A}_q^2]_{u,v} & \dots & e^{i2L\pi} [\mathbf{A}_q^L]_{u,v} \end{pmatrix}, \tag{13}$$

where  $\mathbf{F}_q = (1, \exp\{i4\pi\}, \exp\{i8\pi\}, \dots, \exp\{i8L\pi\}) \in \mathbb{R}^{1 \times (L+1)}$ . Let  $\vec{q} = (q_1, q_2, \dots, q_{L+1})$  with each  $q_j \leq 1/2$  and  $q_j$  are distinct, we can build similar equations for each  $q_j$  and put them into one matrix equation as follows:

$$\mathbf{F}_{\vec{q}} \begin{pmatrix} \Phi_{u,v}(1, 0) & \Phi_{u,v}(2, 0) & \dots & \Phi_{u,v}(L, 0) \\ \Phi_{u,v}(1, 1) & \Phi_{u,v}(2, 1) & \dots & \Phi_{u,v}(L, 1) \\ 0 & \Phi_{u,v}(2, 2) & \dots & \Phi_{u,v}(L, 2) \\ 0 & 0 & \dots & \Phi_{u,v}(L, 3) \\ \dots & \dots & \dots & \Phi_{u,v}(L, L) \end{pmatrix} = \begin{pmatrix} e^{i2\pi} [\mathbf{A}_{q_1}]_{u,v} & \dots & e^{i2L\pi} [\mathbf{A}_{q_1}^L]_{u,v} \\ \dots & \dots & \dots \\ e^{i2\pi} [\mathbf{A}_{q_{L+1}}]_{u,v} & \dots & e^{i2L\pi} [\mathbf{A}_{q_{L+1}}^L]_{u,v} \end{pmatrix}, \tag{14}$$

where  $\mathbf{F}_{\vec{q}} = (\mathbf{F}_{q_1}; \mathbf{F}_{q_2}; \dots; \mathbf{F}_{q_{L+1}}) \in \mathbb{R}^{(L+1) \times (L+1)}$ . Since  $q_j \leq 1/2$  and they are distinct, matrix  $\mathbf{F}_{\vec{q}}$  is full-rank, so we can uniquely determine walk profile  $\Phi_{u,v}$  from the RHS matrix. Notably,  $q_j = \frac{j}{2(L+1)}$  makes  $\mathbf{F}_{\vec{q}}$  **discrete Fourier transform**, a unitary matrix which is invertible by taking its conjugate transpose.

Finally, since eigenvectors and eigenvalues at node  $u, v$  decomposed from  $\mathbf{L}_{\vec{q}}$  (and with some node degree information) allow us to compute  $[\mathbf{A}_{q_j}^\ell]_{u,v}$ , we are able to reconstruct walk profile  $\Phi_{u,v}$ .  $\square$

## B Experimental Setup

In this section, we give further implementation details. We use Quadro RTX 6000 on Linux system to train the models. The training time for single run is typically between 1 hour to 5 hours.

Note that for SignNet, we use  $\phi$  and  $\rho$  to represent  $\text{SignNet}(v_1, \dots, v_d) = \rho([\phi(v_j) + \phi(-v_j)]_{j=1, \dots, d})$ , where  $v_j$  is the  $i$ -th eigenvectors.

For SPE, we use both node SPE  $z_{\text{node}}$  and edge SPE  $z_{\text{edge}}$  by default, except for High-level synthetic task where we find using  $z_{\text{node}}$  only has comparable performance to both  $z_{\text{node}}$  and  $z_{\text{edge}}$ .

For each experiment, the search space for baseline single  $q$  is exactly the range of multiple  $\vec{q}$ . For example, if for multiple  $\vec{q}$  we choose  $\vec{q} = (1/10, 2/10, \dots, 5/10)$ , then for baseline single  $q$  we search over  $q = 1/10, 2/10, \dots, 5/10$ .



| Hyperparameter | walk profile (regular graphs)   | spd (regular graphs)     | lpd (regular graphs)     |
|----------------|---|--------------------------|--------------------------|
| Base model     | 8-layer MLPs  |                          |                          |
| Hidden dim     | 64  |                          |                          |
| Batch size     | 512   |                          |                          |
| Learning rate  | 1e-3  |                          |                          |
| Dropout        | 0   |                          |                          |
| Epoch          | 150   |                          |                          |
| Optimizer      | Adam ( $\beta_1 = 0.9, \beta_2 = 0.999$ )   |                          |                          |
| PE dim         | 32  |                          |                          |
| Multiple q     | (1/10, 2/10, ..., 5/10)   | (1/30, 2/30, ..., 15/30) | (1/30, 2/30, ..., 15/30) |
| PE processing  | SignNet ( $\phi=3$ -layer MLPs, $\rho=3$ -layer MLPs), SPE ( $\phi=3$ -layer MLPs, $\rho=2$ -layer GIN) |                          |                          |

Table 4: Hyperparameter for walk profile/shortest path distance/longest path distance prediction on regular directed graphs.

| Hyperparameter | walk profile (DAG)  | spd (DAG)                | lpd (DAG)                |
|----------------|---|--------------------------|--------------------------|
| Base model     | 8-layer MLPs  |                          |                          |
| Hidden dim     | 64  |                          |                          |
| Batch size     | 512   |                          |                          |
| Learning rate  | 1e-3  |                          |                          |
| Dropout        | 0   |                          |                          |
| Epoch          | 150   |                          |                          |
| Optimizer      | Adam ( $\beta_1 = 0.9, \beta_2 = 0.999$ )   |                          |                          |
| PE dim         | 32  |                          |                          |
| Multiple q     | (1/10, 2/10, ..., 5/10)   | (1/20, 2/20, ..., 10/20) | (1/20, 2/20, ..., 10/20) |
| PE processing  | SignNet ( $\phi=3$ -layer MLPs, $\rho=3$ -layer MLPs), SPE ( $\phi=3$ -layer MLPs, $\rho=2$ -layer GIN) |                          |                          |

Table 5: Hyperparameter for walk profile/shortest path distance/longest path distance prediction on directed acyclic graphs.

## B.1 Distance Prediction on Directed Graphs

### B.1.1 Model Hyperparameter

See Table 4 and 5.

### B.2 Sorting Networks

| Hyperparameter | Sorting Network   |
|----------------|---|
| Base model     | 3-layer Transformer+mean pooling+3-layer MLPs   |
| Hidden dim     | 256   |
| Batch size     | 48  |
| Learning rate  | 1e-4  |
| Dropout        | 0.2   |
| Epoch          | 15 (SignNet) or 5 (SPE)   |
| Optimizer      | Adam ( $\beta_1 = 0.7, \beta_2 = 0.9$ , weight decay $6 \times 10^{-5}$ )                               |
| PE dim         | 25  |
| Multiple q     | (1/20, 2/10, ..., 5/20) / $d_G$   |
| PE processing  | SignNet ( $\phi=3$ -layer MLPs, $\rho=3$ -layer MLPs), SPE ( $\phi=3$ -layer MLPs, $\rho=2$ -layer GIN) |

Table 6: Hyperparameter for sorting network prediction.

### B.2.1 Model Hyperparameter

See Table 6.

### B.2.2 Dataset Generation

Our sorting networks generation follows exactly as [25]. To generate a sorting network, the length of sequence (number of variables to sort) is first randomly chosen. Given the sequence length, each step it will generate a pair-wise sorting operator between two random variables, until it becomes a valid sorting network (can correctly sort arbitrary input sequence) or reaches the maximal number of

| Hyperparameter | Gain   | BW                         | PM                         |
|----------------|--|----------------------------|----------------------------|
| Base model     | 4-layer bidi. GIN  | 3-layer bidi. GIN          | 4-layer bidi. GIN          |
| Graph Pooling  | Sum  | Sum                        | Sum                        |
| Hidden dim     | 96   | 192                        | 288                        |
| Batch size     | 128  | 64                         | 64                         |
| Learning rate  | 0.0067   | 0.0065                     | 0.0021                     |
| Dropout        | 0.1  | 0                          | 0.2                        |
| Epoch          | 300  | 300                        | 300                        |
| Optimizer      | Adam ( $\beta_1 = 0.9, \beta_2 = 0.999$ )  |                            |                            |
| PE dim         | 10   |                            |                            |
| Multiple q     | (1/100, 2/100, ..., 10/100)  | (1/100, 2/100, ..., 5/100) | (1/100, 2/100, ..., 5/100) |
| PE processing  | SignNet ( $\phi=1$ -layer bidi. GIN, $\rho=3$ -layer MLPs), SPE ( $\phi=3$ -layer MLPs, $\rho=2$ -layer bidi. GIN) |                            |                            |

Table 7: Hyperparameter for bidirected GIN on Open Circuit Benchmark.

| Hyperparameter | Gain   | BW                         | PM                         |
|----------------|--|----------------------------|----------------------------|
| Base model     | 4-layer undi. GIN  | 3-layer undi. GIN          | 4-layer undi. GIN          |
| Graph Pooling  | Sum  | Sum                        | Sum                        |
| Hidden dim     | 96   | 192                        | 288                        |
| Batch size     | 128  | 64                         | 64                         |
| Learning rate  | 0.0067   | 0.0065                     | 0.0021                     |
| Dropout        | 0.1  | 0                          | 0.2                        |
| Epoch          | 300  | 300                        | 300                        |
| Optimizer      | Adam ( $\beta_1 = 0.9, \beta_2 = 0.999$ )  |                            |                            |
| PE dim         | 10   |                            |                            |
| Multiple q     | (1/100, 2/100, ..., 10/100)  | (1/100, 2/100, ..., 5/100) | (1/100, 2/100, ..., 5/100) |
| PE processing  | SignNet ( $\phi=1$ -layer undi. GIN, $\rho=3$ -layer MLPs), SPE ( $\phi=3$ -layer MLPs, $\rho=2$ -layer undi. GIN) |                            |                            |

Table 8: Hyperparameter for undirected GIN on Open Circuit Benchmark.

| Hyperparameter | Gain   | BW                            | PM                            |
|----------------|--|-------------------------------|-------------------------------|
| Base model     | 3-layer SAT (2-hop bidi. GIN)  | 3-layer SAT (2-hop bidi. GIN) | 3-layer SAT (1-hop bidi. GIN) |
| Graph Pooling  | Sum  | Sum                           | Sum                           |
| Hidden dim     | 54   | 78                            | 54                            |
| Batch size     | 256  | 256                           | 64                            |
| Learning rate  | 0.004  | 0.00119                       | 0.00117                       |
| Dropout        | 0.2  | 0.3                           | 0.2                           |
| Epoch          | 200  | 200                           | 200                           |
| Optimizer      | Adam ( $\beta_1 = 0.9, \beta_2 = 0.999$ )  |                               |                               |
| PE dim         | 10   |                               |                               |
| Multiple q     | (1/100, 2/100, ..., 5/100)   | (1/100, 2/100, ..., 10/100)   | (1/100, 2/100, ..., 5/100)    |
| PE processing  | SignNet ( $\phi=1$ -layer bidi. GIN, $\rho=3$ -layer MLPs), SPE ( $\phi=3$ -layer MLPs, $\rho=2$ -layer bidi. GIN) |                               |                               |

Table 9: Hyperparameter for SAT (each layer uses bidirected GIN as kernel) on Open Circuit Benchmark.

sorting operators. The resulting sorting network is then translated into a directed graph, where each node represents a sorting operator, whose feature is the ids of two variables to sort. In the sorting network, if two sorting operators share a common variable to sort, the corresponding nodes will be connected by a directed edge (from the first operator to the second one).

For each generated sorting network, the test dataset further contains the reversion version of the graph, by reversing every directed edge in the directed graph. The resulting reverse sorting network is very likely not a valid sorting network.

### B.3 Open Circuit Benchmark

### B.4 Bi-level GNN

Note that graphs in the dataset are two-level: some directed edges describe the connection of nodes (regular edges), while some extra edges represent subgraph patterns in the graph (subgraph edges). In our experiment, we uniform apply a GNN to the nodes with subgraph edges only, and then apply other GNN to the nodes with regular edges.

| Hyperparameter | Gain   | BW                            | PM                            |
|----------------|--|-------------------------------|-------------------------------|
| Base model     | 3-layer SAT (1-hop undi. GIN)  | 3-layer SAT (1-hop bidi. GIN) | 3-layer SAT (1-hop bidi. GIN) |
| Graph Pooling  | Sum  | Sum                           | Sum                           |
| Hidden dim     | 54   | 54                            | 54                            |
| Batch size     | 64   | 256                           | 64                            |
| Learning rate  | 0.009  | 0.002                         | 0.00117                       |
| Dropout        | 0.2  | 0.3                           | 0.1                           |
| Epoch          | 200  | 200                           | 200                           |
| Optimizer      | Adam ( $\beta_1 = 0.9, \beta_2 = 0.999$ )  |                               |                               |
| PE dim         | 10   |                               |                               |
| Multiple q     | (1/100, 2/100, ..., 10/100)  | (1/100, 2/100, ..., 10/100)   | (1/100, 2/100, ..., 10/100)   |
| PE processing  | SignNet ( $\phi=1$ -layer undi. GIN, $\rho=3$ -layer MLPs), SPE ( $\phi=3$ -layer MLPs, $\rho=2$ -layer undi. GIN) |                               |                               |

Table 10: Hyperparameter for SAT (each layer uses undirected GIN as kernel) on Open Circuit Benchmark.

| Hyperparameter | Gain   | BW                         |
|----------------|--|----------------------------|
| Base model     | 4-layer bidi. GIN  | 4-layer bidi. GIN          |
| Graph Pooling  | Mean   | Mean                       |
| Hidden dim     | 84   | 192                        |
| Batch size     | 64   | 56                         |
| Learning rate  | 0.003  | 0.0023                     |
| Dropout        | 0.2  | 0.1                        |
| Epoch          | 400  | 400                        |
| Optimizer      | Adam ( $\beta_1 = 0.9, \beta_2 = 0.999$ )  |                            |
| PE dim         | 10   |                            |
| Multiple q     | (1/100, 2/100, ..., 5/100)   | (1/100, 2/100, ..., 5/100) |
| PE processing  | SignNet ( $\phi=2$ -layer bidi. GIN, $\rho=3$ -layer MLPs), SPE ( $\phi=3$ -layer MLPs, $\rho=2$ -layer bidi. GIN) |                            |

Table 11: Hyperparameter for bidirected GIN on High-level Synthetic dataset.

| Hyperparameter | Gain   | BW                         |
|----------------|--|----------------------------|
| Base model     | 2-layer undi. GIN  | 4-layer bidi. GIN          |
| Graph Pooling  | Mean   | Mean                       |
| Hidden dim     | 56   | 84                         |
| Batch size     | 32   | 32                         |
| Learning rate  | 0.006  | 0.0015                     |
| Dropout        | 0.1  | 0.3                        |
| Epoch          | 400  | 400                        |
| Optimizer      | Adam ( $\beta_1 = 0.9, \beta_2 = 0.999$ )  |                            |
| PE dim         | 10   |                            |
| Multiple q     | (1/100, 2/100, ..., 5/100)   | (1/100, 2/100, ..., 5/100) |
| PE processing  | SignNet ( $\phi=2$ -layer undi. GIN, $\rho=3$ -layer MLPs), SPE ( $\phi=3$ -layer MLPs, $\rho=2$ -layer undi. GIN) |                            |

Table 12: Hyperparameter for undirected GIN on High-level Synthetic dataset.

#### B.4.1 Model Hyperparameter

See Table 7, 8, 9, 10.

### B.5 High-level Synthetic

#### B.5.1 Model Hyperparameter

See Table 11, 12, 13, 14.

## C Varying Single $q$ Baseline

This section shows the effect the varying single  $q$  on the performance of Mag-PE. Horizontal axis is the value of single  $q$ , vertical axis is the test performance. The dashed line represents the result of Multi- $q$  Magnetic Laplacian with fixed multi- $q$   $\vec{q}$  as described in Section 5.1.

As shown in Figures 4, 5, 6, 7, we can see that the multiple  $q$  performance consistently beats best performance of single  $q$ , which demonstrates the benefits of using multiple  $q$  simultaneously.

| Hyperparameter | Gain   | BW                            |
|----------------|--|-------------------------------|
| Base model     | 4-layer SAT (2-hop bidi. GIN)  | 3-layer SAT (2-hop bidi. GIN) |
| Graph Pooling  | Mean   | Mean                          |
| Hidden dim     | 78   | 62                            |
| Batch size     | 64   | 64                            |
| Learning rate  | 0.004  | 0.004                         |
| Dropout        | 0.1  | 0.1                           |
| Epoch          | 400  | 400                           |
| Optimizer      | Adam ( $\beta_1 = 0.9, \beta_2 = 0.999$ )  |                               |
| PE dim         | 10   |                               |
| Multiple q     | (1/100, 2/100, ..., 5/100)   | (1/100, 2/100)                |
| PE processing  | SignNet ( $\phi=2$ -layer bidi. GIN, $\rho=3$ -layer MLPs), SPE ( $\phi=3$ -layer MLPs, $\rho=2$ -layer bidi. GIN) |                               |

Table 13: Hyperparameter for SAT (each layer uses bidirected GIN as kernel) on High-level Synthetic dataset.

| Hyperparameter | Gain   | BW                            |
|----------------|--|-------------------------------|
| Base model     | 3-layer SAT (2-hop bidi. GIN)  | 3-layer SAT (2-hop bidi. GIN) |
| Graph Pooling  | Mean   | Mean                          |
| Hidden dim     | 98   | 62                            |
| Batch size     | 64   | 64                            |
| Learning rate  | 0.004  | 0.004                         |
| Dropout        | 0.1  | 0.1                           |
| Epoch          | 400  | 400                           |
| Optimizer      | Adam ( $\beta_1 = 0.9, \beta_2 = 0.999$ )  |                               |
| PE dim         | 10   |                               |
| Multiple q     | (1/100, 2/100, ..., 5/100)   | (1/100, 2/100, ..., 5/100)    |
| PE processing  | SignNet ( $\phi=2$ -layer bidi. GIN, $\rho=3$ -layer MLPs), SPE ( $\phi=3$ -layer MLPs, $\rho=2$ -layer bidi. GIN) |                               |

Table 14: Hyperparameter for SAT (each layer uses undirected GIN as kernel) on High-level Synthetic dataset.

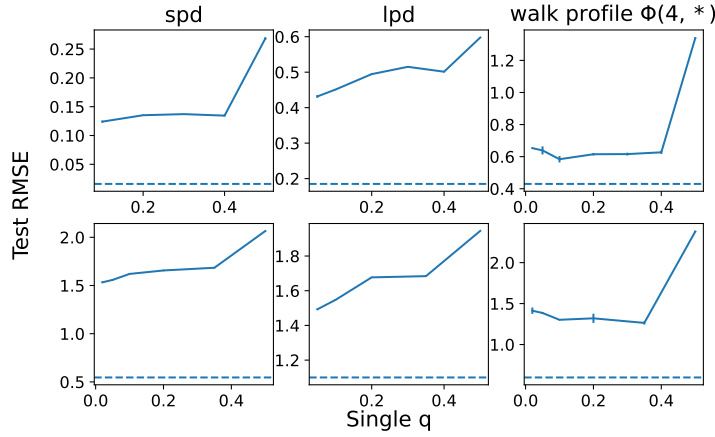


Figure 4: Test RMSE for distance prediction with varying  $q$  of single- $q$  Magnetic Laplacian. First row is for directed acyclic graphs, and second row is for regular directed graphs.

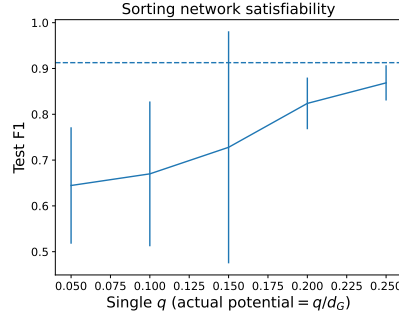


Figure 5: Test F1 of sorting network satisfiability with varying single  $q$ .

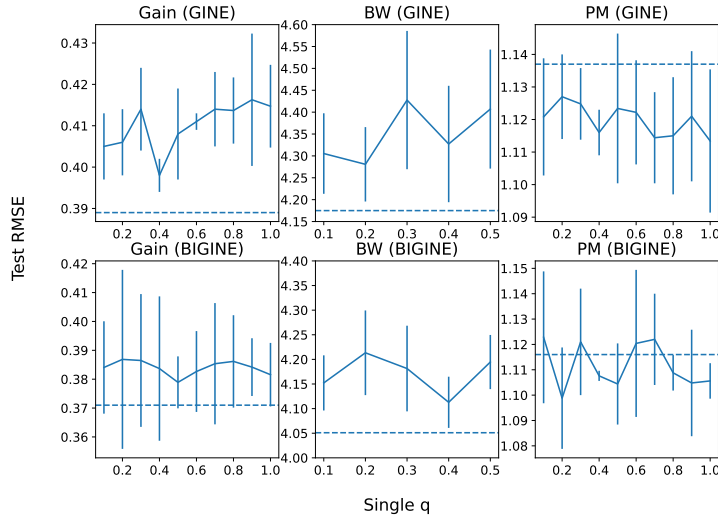


Figure 6: Test RMSE for prediction of Gain, BW, PM using backbone GINE or BIGINE, with varying  $q$  of single- $q$  Magnetic Laplacian.

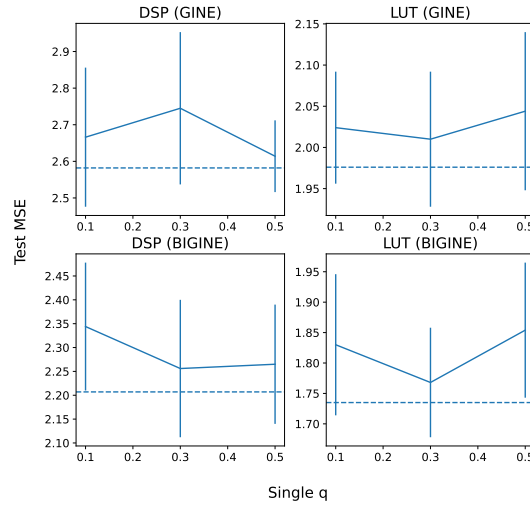


Figure 7: Test MSE for prediction of DSP and LUT, using backbone GINE or BIGINE, with varying  $q$  of single- $q$  Magnetic Laplacian.